International Journal of Nanoelectronics and Materials
IJNeaM
ISSN 1985-5761 | E-ISSN 2232-1535

Elaboration of Fe_3O_4/ZnO-C hybrid nanocomposites with highly photoluminescence intensity

Astuti[a]*, Syukri Arief[b], Mulda Muldarisnur[a], Zulhadjri[b]

[a]*Department of Physics, Andalas University, Indonesia*
[b]*Department of Chemistry, Andalas University, Indonesia*
** Corresponding author. Tel.: +62-85263301026; e-mail: astuti@unand.ac.id*

Received 3 March 2025, Revised 27 March 2025, Accepted 24 April 2026

ABSTRACT

This study underscores the role of nanocarbons in enhancing the photoluminescence (PL) of Fe_3O_4/ZnO nanocomposites and their potential applications in biomedicine. As previously known, the PL intensity of ZnO decreased due to the quenching effect by Fe_3O_4. This study investigated the effect of carbon addition on the crystal structure, photoluminescence, and magnetic properties of the nanocomposites. Four nanocarbon mass variations, i.e., 0.2, 0.1, 0.05, and 0.03 g, were used to synthesize the Fe_3O_4/ZnO-C nanocomposites. The X-ray diffraction (XRD) measurements of the nanocomposites displayed Fe_3O_4, ZnO, and carbon phase structures with no impurities. The transmission electron microscopy (TEM) images and fast Fourier transform (FFT) analysis confirm that the ZnO crystals and carbon covered the Fe3O4 nanoparticles. The Fourier transform infrared spectroscopy (FTIR) analysis reported a C-O absorption peak, corresponding to the hybridization between carbon and the Fe_3O_4/ZnO nanocomposites. The VSM data indicated that higher carbon concentration led to lower magnetic saturation. Likewise, PL measurements reported that adding a small amount (0.05 g) of carbon could significantly increase PL intensity. The strongest light emission was found with 0.05 g of carbon, showing the brightest orange light at a wavelength of 660 nm; the magnetic saturation measured 22.05 emu/g, and the crystallite size obtained was 21.36 nm for Fe_3O_4 nanoparticles and 21.34 nm for ZnO nanoparticles. The composition of 0.05 g carbon is the optimum value for producing photoluminescence and magnetic properties for biomedical applications. Therefore, the optical and magnetic properties of the Fe_3O_4/ZnO nanocomposite could be adjusted by surface modification with carbon to improve their application in imaging, diagnostics, and cancer treatment.

Keywords: *Photoluminescence, Nanocomposites, Fe_3O_4/ZnO, Carbon, Bioimaging.*

1. INTRODUCTION

Over the last decade, many studies have focused on Fe_3O_4-based composites for biomedical applications (i.e., diagnosis, imaging, and therapy) due to their biocompatibility, ease of synthesis, and compatibility with other materials composites [1-2]. Several studies have also integrated different materials, polymers [3], folic acid [4], chitosan [5], and silica [6] into Fe_3O_4-based composites to improve their stability and biocompatibility for bioimaging applications. In most multimodal biomedical applications, a combination of Fe_3O_4 magnetic materials and luminescent materials is required [7]. For example, lanthanides [8], semiconductors [9, 10], and carbon-derived materials graphene have been used for luminescence [11]. Among the luminescent materials, zinc oxide (ZnO) is particularly interesting as it is a non-toxic substance with no indication of carcinogenicity, genotoxicity, or reproduction toxicity. In addition, it has good biocompatibility and, thus, may be employed for biological applications [12].

Several researchers have reported surface modifications of ZnO to increase its photoluminescence (PL) intensity. For example, rare earth ion doping improved the PL of ZnO [13], but rare earths are unsuitable for biomedical applications due to their toxicity. As an alternative, ZnO was modified with various carbon allotropes to obtain a novel hybridized structure with PL intensity that could be modulated. Some examples like carbon black-hybridized ZnO quantum dots (QDs) [14], graphene-embedded ZnO film [20], carboxylate-capped ZnO QDs [15], and carbon decorated T-ZnO have enhanced PL properties [16]. Hence, the effective combination of the magnetic material Fe_3O_4 and ZnO presents a potentially effective biomedical material [13]. The synthesis of Fe_3O_4/ZnO nanocomposites has been extensively studied. However, research on their application as a bioimaging material requires further investigation into the quenching effect of Fe on ZnO, which reduces the luminescence intensity of ZnO. Likewise, only a few studies have investigated an easy in-situ growing method to remarkably enhance the visible PL intensity of Fe_3O_4/ZnO for medical applications.

This study synthesized a hybrid nanocomposite of Fe_3O_4/ZnO and nanocarbon material with enhanced PL and magnetic properties. Fe_3O_4/Zno was synthesized using the coprecipitation method. The focus of this research was to reduce PL quenching by Fe_3O_4 on ZnO and increase Fe_3O_4/ZnO PL by passivating the ZnO surface to reduce agglomeration using nanocarbon. Previous studies have not determined the optimal amount of nanocarbon required to achieve photoluminescent and magnetic properties in Fe_3O_4/ZnO. Therefore, this study emphasizes

the optimum amount of carbon needed to obtain suitable biomedical applications. Surface properties were also studied for their effect on the functional properties of ZnO in Fe_3O_4/ZnO nanocomposites. This article reported that adding small carbon atoms increased the PL intensity of the hybrid Fe_3O_4/ZnO-C nanocomposites.

2. METHODOLOGY

Fe_3O_4/ZnO nanocomposites were synthesized using iron (III) chloride hexahydrate ($FeCl_3.6H_2O$, Merck), iron (II) sulfate heptahydrate ($FeSO_4.7H_2O$), zinc nitrate ($ZnO(NO_3)_2$), ammonium hydroxide (NH_4OH, 21% NH_3) were obtained from Merck. Carbon was synthesized using polyethylene glycol (PEG), and glucose was the product of Bratachem, Indonesia. Aquadest and 96% alcohol were obtained from Bratachem, Indonesia.

2.1. Fe_3O_4/ZnO Nanocomposite Synthesis

The Fe_3O_4/ZnO nanocomposite was synthesized based on our previous protocol [17], which modified the method reported by Madhubala and Kailavani [8]. In order to create the Fe_3O_4 composites, 30 mL of aquadest (distilled water) was used to dissolve $FeSO_4.7H_2O$ and $FeCl_3.6H_2O$ in a molar ratio of 1:2. The solution turned solid black when 30 mL of NH_4OH were added gradually to the homogeneous solution, and reach PH 11. A magnetic stirrer agitated the solution for 120 minutes at 60 °C. A permanent magnet was used to precipitate the solution, and then the precipitate was washed three times using aquadest. Fe_3O_4 nanoparticles that have been formed were coated with ZnO nanoparticles. The steps for coating Fe_3O_4 with ZnO were as follows: 30 mL of NH_4OH were added after dissolving zinc nitrate ($ZnO(NO_3)_2$) in 100 mL of aquadest. After mixing the $ZnO(NO_3)_2$ solution with the Fe_3O_4 precipitate, it was agitated for 24 hours at 70 °C using a magnetic stirrer. After precipitating and separating from the solvent, the solution underwent three rounds of washing. After drying at 300 °C in a furnace for two hours, the precipitate was crushed with a crusher and pestle to create Fe_3O_4/ZnO powder.

2.2. Coupling of Carbon with Fe_3O_4/ZnO Nanocomposite

The hybrid Fe_3O_4/ZnO-C nanocomposite was synthesized using our previous protocol [18]. Pure carbon was first extracted before coupling with the Fe_3O_4/ZnO nanocomposite. A digital analytical scale weighed 0.53 g of PEG and 1.8 g of glucose (1:2), which were then dissolved in 25 ml of aquadest. After that, the solution was agitated for 30 minutes at 450 rpm using a magnetic stirrer. The solution was dried in an oven set to 300 °C for three hours to get pure carbon. The carbon was then ground until it was smooth. After that, 10 milliliters of aquadest were mixed with 0.2 grams of carbon powder. To create very fine Fe_3O_4/ZnO-C powder, 0.4 g of the powder was then added to the carbon solution, agitated with a magnetic stirrer for 1 hour at 90 °C, and dried for 3 hours at 250 °C. Further synthesis was conducted with the same procedure.

2.3 Instrumentation

A wide range of methods and approaches defines nanostructure. In general, there are two procedures in nanostructural characterization, namely chemical and morphological characterization. Fe_3O_4/ZnO-C nanocomposite characterization in this report includes characterization of the crystal structure using X-ray diffraction (XRD) measurement (Bruker D8 Advance). The diffractogram was obtained by using Cu-Kα radiation (λ = 1.5406 Å) in the range 10°<2θ°<100° with steps of 0.02°. The morphology of the samples was analyzed using transmission electron microscopy (TEM) technique (FEI Tecnai G2 20 S-Twin), while PL analysis was investigated using Horiba MicOS PL Microspectrometer. Photoluminescence spectra were obtained using an excitation wavelength of 325 nm. Determining functional groups using Fourier transform infrared spectroscopy (FTIR) (Nicolet iS50). These measurements were performed in the frequency interval of 4000–400 cm^{-1} with a resolution of 1.29 cm^{-1}. Analyzing magnetic properties using VSM (VSM250). The measurements were taken at room temperature (25 °C) and under different applied magnetic fields from −7 to +7 kOe.

3. RESULTS AND DISCUSSION

3.1. XRD Analysis

The different concentrations of carbon in Fe_3O_4/ZnO-C nanocomposites were analyzed with XRD in terms of their structure and crystallinity. XRD results of Fe_3O_4 nanoparticles, Fe_3O_4/ZnO, and Fe_3O_4/ZnO-C nanocomposites are displayed in Figure 1. The Fe_3O_4 diffraction data was compared to the ICDD standard data with reference code 01-088-0315. The diffraction peaks with Miller indices (220), (311), (400), (442), (511), (440), and (533) corresponded to 2θ of 30.16°, 35.56°, 43.14°, 53.58°, 57.15°, 62.85°, and 74.16°, respectively. The Fe_3O_4 crystal structure was cubic, with lattice parameters a = b = c = 8.37 Å. Meanwhile, ZnO has lattice constants around a = b = 3.25 Å and c = 5.21 Å (ICDD, reference code 01-089-7102). The peaks at around 31.74°, 34.42°, 36.25°, 47.61°, 56.77°, and 62.97° correspond to the (100), (002), (101), (102), (103), (112), and (201) ZnO planes, based on the JCPDS 01-089-7102, confirming the typical ZnO hexagonal wurtzite structure.

XRD pattern for Fe_3O_4/ZnO nanocomposites showed that impurity-free Fe_3O_4 and ZnO phases formed. According to these data, the crystal structure and lattice parameters of the Fe_3O_4 phase did not change. XRD data for the Fe_3O_4/ZnO-C nanocomposite revealed the formation of three phases, namely Fe_3O_4, ZnO, and C (graphitic). Neither Fe_3O_4 nor ZnO exhibited changes in the crystal structure, namely cubic and hexagonal wurtzite, but there was a slight change in the ZnO lattice parameters, namely a = b = 3.24 Å and c = 5.17 Å. Decreased crystallite size correlates with a drop in a lattice parameter.

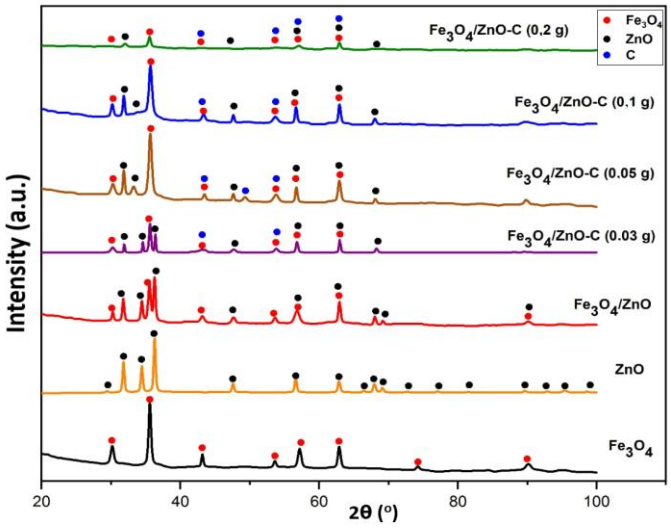

Figure 1. The diffraction pattern of Fe_3O_4, Fe_3O_4/ZnO, Fe_3O_4/ZnO-C (0.03 g), Fe_3O_4/ZnO-C (0.05 g), Fe_3O_4/ZnO-C (0.1 g), and Fe_3O_4/ZnO-C (0.2 g).

The decrease is because smaller crystallites tend to have higher lattice defects or strain concentrations, which are frequently indicated by a smaller lattice parameter. According to reference number 01-073-5918, the carbon phase was identified with a rhombohedral crystal structure. Based on XRD data, it is known to have a lattice constant a = b = 2.51 Å and c = 10.20Å. Every Fe_3O_4 phase exhibited a cubic crystal structure, including Fe_3O_4/ZnO-C nanocomposites containing 0.2, 0.1, 0.05, and 0.03 g of carbon. Likewise, ZnO had a hexagonal wurtzite crystal structure in all samples [17, 18].

No changes were observed in the lattice constant of the Fe_3O_4 phase for all samples. However, there was a slight decrease in the lattice constant in the ZnO crystals in the Fe_3O_4/ZnO-C nanocomposite. The shrinkage of the lattice constant is caused by the presence of carbon on the ZnO surface. The diffraction peak at the Miller index (101) was absent when the amount of carbon added to the Fe_3O_4/ZnO-C nanocomposites was increased (i.e., 0.05, 0.1, and 0.2 g). The addition of carbon affected the PL of ZnO (Figure 4). In the Fe_3O_4/ZnO-C nanocomposite (0.05 g), a carbon diffraction peak was visible at 2θ = 49.28°, corresponding to the Miller index (102). In the Fe_3O_4/ZnO-C nanocomposite (0.2 g), there were more carbon diffraction peaks corresponding to the increased carbon content in the composite. The decrease in the diffraction peak in the 0.2 g carbon sample was caused by a decrease in crystallinity, which can be seen from the decrease in crystal size, as shown in Table 1. Increasing the amount of carbon can decrease long-range crystal order since it can result in lattice strain and defect states. The decrease in the diffraction peak in the 0.03 g carbon sample was likely caused by dislocations in the Fe_3O_4/ZnO crystals [8,9]. The calculation of crystal size using the Scherrer equation (1) can be written as,

$$D = \frac{K\lambda}{\beta \cos\theta} \quad (1)$$

The nano crystallite size (D) was determined using the Scherrer equation and XRD radiation with a wavelength of λ (nm). The calculation was done by measuring the whole width at half maximum of peaks (β) in radians at any 2θ in the pattern. Typically, K's form factor is estimated to be around 0.89. The crystal size for each sample is displayed in Table 1.

Table 1. Crystal sizes of the Fe_3O_4 and ZnO phases for each sample variation.

Samples	D (Fe_3O_4 (nm))	D (ZnO (nm))
Fe_3O_4	16.39	-
ZnO	-	23.27
Fe_3O_4/ZnO	20.61	23.21
Fe_3O_4/ZnO-C (0.2 g)	20.67	20.39
Fe_3O_4/ZnO-C (0.1 g)	21.31	21.34
Fe_3O_4/ZnO-C (0.05 g)	21.36	21.34
Fe_3O_4/ZnO-C (0.03 g)	24.19	23.26

There was a slight increase in the crystal size of Fe_3O_4 and ZnO after adding carbon (Table 1). Carbon addition also decreased the diffraction intensity in the Fe_3O_4 phase and suppressed some ZnO peaks. The decrease in intensity indicated that the carbon effectively coated the Fe_3O_4/ZnO surface. Furthermore, no peaks between Fe_3O_4 and ZnO or other oxide bonds were observed in the XRD pattern, which confirmed the formation of a pure Fe_3O_4/ZnO-C nanocomposite structure.

3.2. TEM Analysis

TEM images of the Fe_3O_4/ZnO-C (0.2 g) nanocomposite were taken to observe the morphology of the nanocomposite [Figures 2(a) and (b)]. Fe_3O_4 and ZnO nanoparticles were spherical with a 15-24 nm diameter. In contrast, carbon particles had a nanorod shape of 7–10 nm diameter. The Fe_3O_4 nanocomposite had a well-defined crystalline with a lattice spacing of d = 0.29 nm (Miller index: 220), and the ZnO composite had a lattice spacing of d = 0.28 nm (Miller index: 100) (Figure 2c). Figure 2 (d) show the FFT analysis of Fe_3O_4/ZnO-C. Fe_3O_4 and ZnO had high crystallinity, which could be inferred from the sharp Fe_3O_4 and ZnO peaks in the diffractogram, whereas carbon displayed low crystallinity [16].

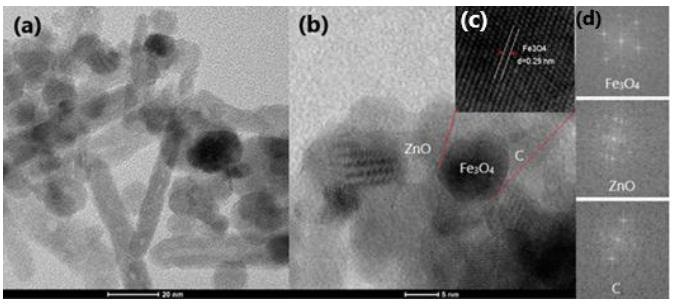

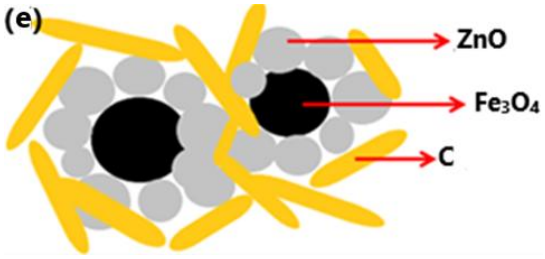

Figure 2. TEM images of the Fe_3O_4/ZnO-C (0.2 g) nanocomposites (a-b), d-spacing of Fe_3O_4 (c), Fast Fourier Transform (FFT) analysis (d), and Illustration of the morphology of Fe_3O_4/ZnO-C (0.2 g) nanocomposite (e).

An illustration of the morphology of the Fe_3O_4/ZnO-C nanocomposite (0.2 g) is shown in Figure 2e. ZnO and carbon particles surround fe_3O_4 particles in the form of nanorods. This morphological structure supports the application of Fe_3O_4/ZnO-C nanocomposites as biomedical materials. The carbon in the outermost layer also functions as a biocompatible layer and maintains the dispersibility of the nanocomposite in water.

3.3. FTIR Analysis

FTIR was measured at 400–4500 cm^{-1} for Fe_3O_4/ZnO and Fe_3O_4/ZnO-C (0.2 g) nanocomposites. The FTIR spectra of the Fe_3O_4/ZnO and Fe_3O_4/ZnO-C nanocomposites are displayed in Figure 3. The Fe_3O_4/ZnO nanocomposite exhibited an O-H group at a wavenumber of 3392.79 cm^{-1}. The absorption peak indicated hydrogen bonds were formed on the Fe_3O_4 surface [19]. The absorption at 400–500 cm^{-1} denoted Zn-O bonds. The formation of Fe_3O_4 was confirmed by the presence of Fe-O bonds at 524.64 and 619.15 cm^{-1} [20, 21]. The FTIR spectrum of Fe_3O_4/ZnO-C looks slightly different from the spectrum of Fe_3O_4/ZnO. The Fe_3O_4/ZnO-C (0.2 g) nanocomposite peaked at 2945.30 cm^{-1}, corresponding to a C-H bond formed in the nanocomposite. Furthermore, the vibrational modes appearing at 1702 and 3408 cm^{-1} in the Fe_3O_4/ZnO-C (0.2 g) correspond to the symmetric stretching of –COOH and symmetric stretching of OH, indicating the presence of carbon at the nanocomposite surface [20]. The C–C vibration appeared as a peak at 1653.64 cm^{-1}. There were octahedral Fe-O bonds at the peak of 524.64 cm^{-1}. The vibrations of the Zn-O bond occurred at 416.62 and 445.56 cm^{-1}.

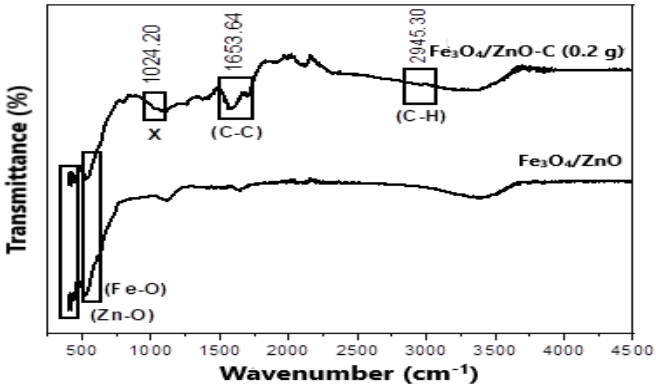

Figure 3. The FTIR spectra of Fe_3O_4/ZnO and Fe_3O_4/ZnO-C (0.2 g).

In addition, a new peak (labeled as X) was identified at 1024.20 cm^{-1}, which could denote the interaction between carbonyl moieties of C with O from the Fe_3O_4/ZnO nanocomposite. The absorption with lower energy than the C-H bond identified at 2945.30 cm^{-1} could justify the interaction. This prediction could be validated because the wavenumber is proportional to the inverse square of the reduced mass (μ). In this regard, we could approximate the C-O bond as follows:

$$\omega_{C-O} = \omega_{C-H}\sqrt{\frac{\mu_{C-H}}{\mu_{C-O}}} \qquad (2)$$

By inserting the appropriate parameter values in equation (2), the estimated $\omega_{(C\text{-}O)}$ was 1061.94 cm^{-1}. The $\omega_{(C\text{-}O)}$ that we obtained was relatively close to the X peak at 1024.20 cm^{-1}. The C-O, C-H, and O-H bonds indicated that a carbon originating from glucose was present. Likewise, the C-O bond indicated hybridization occurred between carbon and the Fe_3O_4/ZnO nanocomposite. The observed peaks validated the successful hybridization of C to the Fe_3O_4/ZnO nanocomposites.

3.4. PL Analysis

The PL spectra for all samples are displayed in Figure 4. Photoluminescence spectra were obtained using an excitation wavelength of 325 nm. There were two emission peaks: a narrow UV emission peak and a broad visible light emission peak ranging from 500 to 800 nm. The optical activity of ZnO's intrinsic defects, which produced near-band edge (NBE) excitons, was shown by the UV emission peak (E = 3.4 eV). On the other hand, the visible light emission showed the presence of ZnO defects and correlated with the electron transition in deep-level emission (DLE). Defects can form during the synthesis of nanocomposites, especially defects on the surface of ZnO, including oxygen vacancies (Vo), Zn vacancies (VZn), oxygen interstitial (O_i) and anti-sites (OZn), and Zn interstitial (Zn_i) [19]. All samples' emission peak characteristics were relatively similar, indicating a similar PL mechanism. DLE is caused by permissible levels within the ZnO band gap that produce transitions with energies in the visible range of the light spectrum. The broad emission band observed in the visible light region was due to the superposition of emissions resulting from several electron transitions [19]. Band broadening in the visible light region started from the blue, yellow, orange, and red emission peaks, which corresponded to wavelengths of 410 nm (E = 3.0 eV), 620 (E = 2.1 eV), 660 (E =1.9 eV), and 760 nm (E = 1.6 eV), respectively. Band broadening is often caused by interstitial oxygen (O_i) and interstitial zinc (Zn_i). The transition between the Zni and Oi levels happened at around 1.9 eV, leading to an orange emission because the interstitial level was 0.22 eV below the conduction band. [22, 23].

The differences between the Fe_3O_4/ZnO-C nanocomposite DLE emission bands for all carbon concentrations (0.03,

0.05, 0.1, and 0.2 g) are also displayed in Figure 4. Generally, there was an increase in PL intensity in the presence of carbon. However, adding 0.05 g of carbon significantly increased the PL intensity of Fe_3O_4/ZnO-C compared to 0.2, 0.1, and 0.03 g of added carbon. Therefore, the findings suggested that 0.05 g of carbon is the optimum amount required to increase the recombination rate of electrons and holes by transferring photoexcited electrons from carbon to the defect level. Electrons moved to various defect levels recombine with holes in the valence band, boosting PL emissions [24]. By increasing the carbon concentration from 0.03 g to 0.05 g, ZnO may develop localized defect states that change the wavelength and intensity of photoluminescence by acting as trap states or radiative recombination centers. However, increasing amounts of carbon could reduce the PL intensity due to the quenching effect of carbon. Quenching happens as a result of processes that non-radiatively eliminate excited state energy. Deep-level traps may be introduced by carbon atoms on the ZnO surface. By increasing non-radiative recombination, these traps lower PL. Energy transmission between nearby luminous centers results in non-radiative routes at high carbon concentrations.

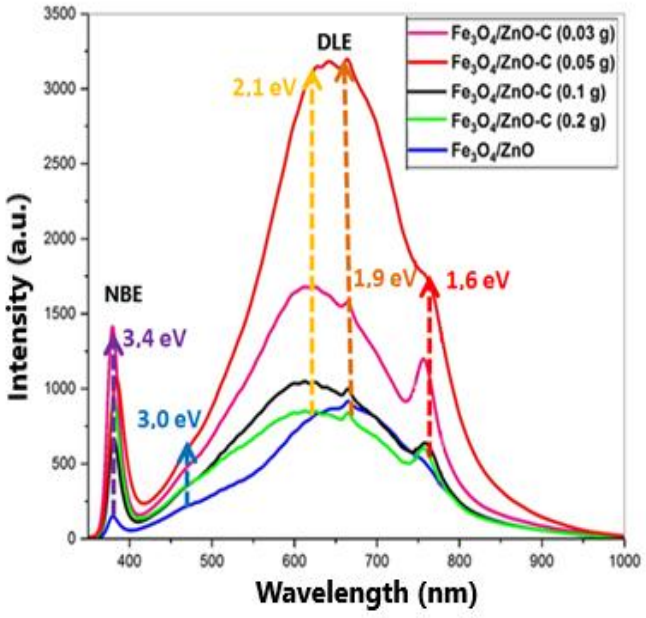

Figure 4. PL spectra of Fe_3O_4/ZnO and Fe_3O_4/ZnO-C nanocomposites.

Another difference identified in the DLE emission band was the emergence of a new peak, red emission in the PL spectrum of Fe_3O_4/ZnO-C around 750–760 nm (1.6 eV), which could also be associated with carbon [25]. The sp^2 domains of the π-π* transition and n-π* transition on the surface functional groups were responsible for the two notable absorption peaks of carbon at 450 and 510 nm, respectively [16, 26-29]. PL and electron-hole pair recombination are intimately associated. Thus, it could be concluded that the higher PL intensities resulted in faster recombination of electron-hole pairs and vice versa.

3.5. VSM Analysis

VSM characterization of Fe_3O_4/ZnO-C nanocomposites was performed at room temperature (Figure 5). All samples exhibited narrow hysteresis curve areas. Particles can spontaneously change their orientation, resulting in near-zero remanence and negligible coercivity fields, which are characteristics of superparamagnetic samples [30]. The magnetic saturation (Ms) values of Fe_3O_4 and Fe_3O_4/ZnO were 68.10 and 66.38 emu/g, respectively [4]. The field coercivity (Hc) values for Fe_3O_4 and Fe_3O_4/ZnO were 40.22 Oe and 44.92 Oe, respectively. The Fe_3O_4/ZnO-C coercivity field values for each concentration of carbon nanorod 0.2, 0.1, 0.05, and 0.03 g were 92.29, 92.90, 89.60, and 94.41 Oe, respectively. The magnetic saturation values of Fe_3O_4/ZnO-C nanocomposites with 0.03, 0.05, 0.1, and 0.2 g of carbon were 35.85, 22.05, 19.33, and 18.23 emu/g, respectively.

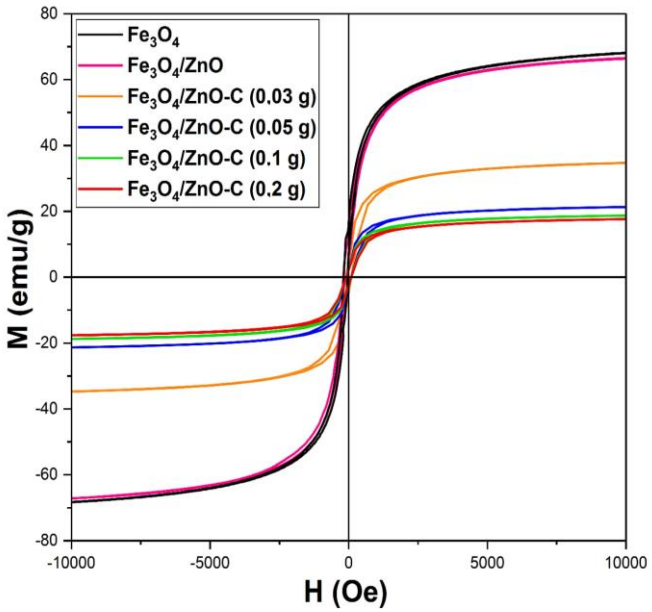

Figure 5. M-H curves of Fe_3O_4, Fe_3O_4/ZnO, and Fe_3O_4/ZnO-C nanocomposites.

As the amount of carbon increased, the magnetic saturation levels dropped. The diamagnetic properties of carbon caused this decrease in magnetic saturation value. Interactions between carbon atoms and Fe_3O_4/ZnO might alter the hybridization of d orbitals, which can impact exchange interactions and inhibit Fe_3O_4's ferromagnetism. In contrast, there was an increase in the coercivity field with increasing carbon content. The increase in coercivity was due to an increase in crystal size; thus, the magnetic moment also increased accordingly. The crystal orientation was not easily influenced by external fields, like pure Fe_3O_4 [31]. The relationship between magnetic properties and crystal size was consistent with the crystal diameter measurements based on XRD characterization in Figure 1 and Table 1. Based on the XRD data, there was an increase in Fe_3O_4 crystal size with increasing carbon content. The measured Ms and Hc values for all samples are displayed in Table 2.

Table 2. VSM measurement results for each sample.

Samples	Ms (emu/g)	Hc (Oe)
Fe_3O_4	68.10	40.22
Fe_3O_4/ZnO	66.38	44.92
Fe_3O_4/ZnO-C (0.03 g)	35.85	94.41
Fe_3O_4/ZnO-C (0.05 g)	22.05	89.60
Fe_3O_4/ZnO-C (0.1 g)	19.33	92.90
Fe_3O_4/ZnO-C (0.2 g)	18.23	92.29

Low magnetic saturation values are preferable to high saturation values for biomedical applications because they reduce tissue damage from strong magnetic fields. Salem et al. also reported a Ms value of approximately 23 emu/g [32]. Likewise, Sabouri et al. obtained MS values of 5–7.88 emu/g for Fe_3O_4-based nanocomposites [33]. A superparamagnetic material with low MS can also be developed for photothermal therapy and drug delivery [34].

4. CONCLUSION

XRD, TEM, and FTIR characterization validated the successful synthesis of Fe_3O_4/ZnO-Carbon nanocomposites using the coprecipitation method. Based on the results of the PL characterization obtained, it can be concluded that adding carbon can significantly increase the photoluminescence intensity. When compared to the photoluminescence intensity without carbon, the photoluminescence intensity was obtained to increase threefold with the addition of 0.05 g of carbon. The emission peak is at the wavelength of visible light that emits bright orange luminescence, namely at a wavelength of 660 nm. The magnetic saturation value decreased with increasing carbon content. Adding 0.05 g of carbon resulted in a magnetic saturation of 22.05 emu/g. This study disclosed that the optical and magnetic properties of Fe_3O_4/ZnO-C nanocomposites could be modulated via surface modification for better biomedical applications, such as bioimaging, diagnostics, and therapy.

ACKNOWLEDGEMENTS

This research was made possible by the supply of research equipment in Andalas University's materials physics laboratory.

REFERENCES

[1] M. Wang, Y. Liang, Z. Zhang, G. Ren, Y. Liu, S. Wu, and J. Shen, "Ag@Fe3O4/ZnO nanoparticles for multimodal imaging-guided chemo-photothermal synergistic targeting for cancer therapy, Analytica Chimica Acta., 1086. pp. 122-132. 2019.

[2] L.Z. Cheng, L.L. Xiang, H.J. Yan, N.Z. Yi, X.X. Yan, Z.L. Yi, L. Cui, "A turn-on colorimetric dual-response fluorescent probe for rapid detecting and its application in bio-imaging and real water samples," Optical Materials., 131, 112625. 2022.

[3] Y. Hu, R. Wang, S. Wang, "Multifunctional Fe3O4/Au core/shell nanostars: a unique platform for multimode imaging and photothermal therapy of tumors", Sci Rep., 6 28325. 2016.

[4] V.M. Thanh, T.H. Nguyen, T.N. Dao, D.T.D. Nguyen V.T and T.N. L. Minh, "Synthesis of ternary Fe3O4/ZnO/chitosan magnetic nanoparticles via an ultrasound-assisted coprecipitation process for antibacterial applications", Journal of Nanomaterials, 2020.

[5] A. Maximenko, J. Depciuch, N. Łopuszynska N, M. Stec, Z. Swiatkowska-Warkocka, V. Bayev ,P.M. Zielinski, J. Baran, J. Fedotova, P. Władysław. We˛glarz and M. Parlinska-Wojta, "Fe3O4@SiO2 @Au nanoparticles for MRI-guided chemo/NIR photothermal therapy of cancer cells", RSC Advances., 10, 26508-26520. 2020.

[6] J. Pellico, C.M Ellis, J.J. Davis, "Nanoparticle-based paramagnetic contrast agents for magnetic resonance imaging," Contrast Media & Molecular Imaging,1–13. 2019

[7] X. Zhao, Q. Yu, J. Yuan, N.V. Thakor and M.C. Tan. "Biodegradable rare earth fluorochloride nanocrystals for phototheranostics," RSC Advance., 10 pp. 15387–15393. 2020.

[8] V. Madhubala, and T. Kalaivani, "Phyto hydrothermal synthesis of Fe3O4/ZnO core-shell nanoparticles using Azadirachta indica and its cytotoxicity studies", Applied Surface Science., 449, pp. 584–590. 2018.

[9] J. Gupta, P.A. Hassan, and K.C. Barick. "Core-shell Fe3O4/ZnO nanoparticles for magnetic hyperthermia and bio-imaging applications", AIP Advances, 11 025207. 2021.

[10] R. Gonzalez-Rodriguez, E. Campbell, A. Naumov, "Multifunctional graphene oxide/iron oxide nanoparticles for magnetic targeted drug delivery dual magnetic resonance/fluorescence imaging and cancer sensing." PLoS ONE, 14 0217072. 2019.

[11] G.A.H. A. Jabbar, A. A. Saeed, M. F. H. AL-Kadhemy, "Optical Characteristics and Antibacterial Activity of PVA/ZnO Nanocomposites" International Journal of Nanoelectronics and Materials, vol. 16, no. 2, pp. 431-440, 2023

[12] M. Reaz, A. Haque, D.M. Cornelison, A. Wanekaya, R. Delong, and K. Ghosh, "Magneto-luminescent zink/iron oxide core-shell nanoparticles with tunable magnetic properties," Physica E: Low-dimensional Systems and Nanostructures 123 114090. 2020.

[13] C.C. Wang, A.Y. Lo, M.C. Cheng, et al., "Zinc oxide nanostructures enhanced photoluminescence by carbon-black nanoparticles in Moiré heterostructures." Sci Rep 13, 9704. 2023

[14] S. Miyashiro C, Hamoudi S, "Palladium and Graphene Oxide Doped ZnO for Aqueous Acetamiprid Degradation under Visible Light." Catalysts. 12(7):709. 2022

[15] J. Duraimurugan, G.S. Kumar, M. Venkatesh, et al.," Morphology and size-controlled Synthesis of zinc oxide nanostructures and their optical properties." J Mater Sci: Mater Electron, 29, pp. 9339–9346. 2018

[16] Astuti, A., Usna, S. "The Influence of Carbon Quantum Dots Addition on the Photoluminescence Performance

of ZnO Nanoparticles," Scientia Iranica, (), pp. -. doi: 10.24200/sci.2024.63810.8610, 2024.

[17] Astuti, S. Arief. Muldarisnur, Zulhadjri, "Synthesis and properties of magnetic-luminescent Fe3O4/ZnO/C nanocomposites", Journal of Nanotechnology, 2023. 2023.

[18] Astuti, S. Arief, Muldarisnur, Zulhadjri, S.R.A. Usna, "Enhancement in photoluminescence performance of carbon-based Fe3O4/ZnO–C nanocomposites". Vacuum, 211, 111935. 2023.

[19] B.L. Zhu, X.M. Cao, M. Xie, J. Wu, X.W. Shi, "Effects of Cu doping and deposition atmosphere on structural, electrical, optical and magnetic properties of ZnO films," Physica B: Condensed Matter, 658,2023.

[20] S. Ahmadian-Fard-Fini, M. Salavati-Niasari, & D. Ghanbari, "Hydrothermal green synthesis of magnetic Fe3O4-carbon dots by lemon and grapefruit extracts and as a photoluminescence sensor for detecting of E. coli bacteria", Spectrochim. Acta. A. Mol. Biomol. Spectrosc 203, pp. 481—493. 2018.

[21] Z. Jia Ng, Y. H. Teow, A. W. Mohammad, K. C. Ho, and S. P. Yeap, "Synthesis of Silica-coated Iron Oxide Nanoparticles: Effect of Particle Sizes and Silica Coating, International," Journal of Nanoelectronics and Materials, vol. 13, no. 3, pp. 565-576, 2020.

[22] S. Pramanik, S. Mukherjee, S. Dey, S. Mukherjee, S. Das, T. Ghosh, P. Ghosh, R. Nath, P K. Kuiri, "Cooperative effects of zinc interstitials and oxygen vacancies on violet-blue photoluminescence of ZnO nanoparticles: UV radiation-induced enhanced latent fingerprint detection," J. Luminescence, 251, 119156, 2022.

[23] A. Galdámez-Martinez, G. Santana, F. Güell, P.R. Martínez-Alanis, A. Dutt "Photoluminescence of ZnO Nanowires", A Review. Nanomaterials. 10(5):857. 2020

[24] Y.J. Park, K.B. Ko, K.S. Lee, T.H. Seo, C.H. Hong, T.V. Cuong, D.I. Son, "Solution-processed graphene quantum dots decorated ZnO nanoflowers for mediating photoluminescence," Applied Surface Science., 510., 145407. 2020.

[25] Nugroho, D., Wannakan, K., Nanan, S. et al. The Synthesis of carbon dots//zincoxide (CDs/ZnO-H400) using hydrothermal methods for degradation of ofloxacin antibiotics and reactive red azo dye (RR141). Sci Rep 14, 2455, 2024.

[26] J. Tang, J. Zhang, Y. Zhang, et al., "Influence of group modification at the edges of carbon quantum dots on fluorescent emission," Nanoscale Res Lett.,14, 241. 2019

[27] K. Suzuki, M. Takahashi, L. Malfatti, and P. Innocenzi, "Carbon dots in ZnO macroporous films with controlled photoluminescence through defects engineering," The Royal Society of Chemistry, 6, pp. 55393-55400. 2016

[28] S.K. Mandal, K. Dutta, S. Pal, S. Mandal, A. Naskar, P.K. Pal, T.S. Bhattacharya, A. Singha, R. Saikh, D. Sukanta, D. Jana, "Engineering of ZnO/rGO nanocomposite photocatalyst towards rapid degradation of toxic dyes," Materials Chemistry and Physics, 223, pp. 456-465. 2019

[29] S. Payrazm., S. Baghshahi, Z. Sadeghian, A. Aliabadizadeh, "Structural and optical characterization of zno-graphene nanocomposite quantum dots," IJMSE., 19, pp. 1-13. 2022

[30] Kim, H, Im, PW, Lee, C, Hong, H, Lee, W, Koo, C, Park, SY, Im, HJ, Paek, SH & Piao, Y, "In vitro magnetic hyperthermia properties of angle-shaped superparamagnetic iron oxide nanoparticles synthesized by a bromide-assisted polyol method," RSC Advances, 13(5), pp. 2803-2810, 2023.

[31] M.R Ghazanfari,., M Kashefi,., S.F Shams,., and M.R Jaafari, "Perspective of Fe3O4 nanoparticles role in biomedical applications". Biochemistry Research International. 32. 2016

[32] M.L Salem, A Gemeay, S Gomaa, M.A. Aldubayan, and I. Assy, "Superparamagnetic graphene oxide/magnetite nanocomposite delivery system for doxorubicin-induced distinguished tumor cell cycle arrest and apoptosis." J. Nanopart Res 22, 219. 2020

[33] Z. Sabouri, F. Karimzadeh, A. Baharlou-Houreh, T.V. McFarlane, M.H Nasr Esfahani, "Fe3O4/bioactive glass nanostructure: a promising therapeutic platform for osteosarcoma treatment". Biomed. Mater 16, 035016. 2021

[34] M Zhang, W. Wang, Y. Cui, X. Chu, B. Sun, N. Zhou, J. Shen, "Magnetofluorescent Fe3O4/carbon quantum dots coated single-walled carbon nanotubes as dual-modal targeted imaging and chemo/photodynamic/photothermal triple-modal therapeutic agents". Chemical Engineering Journal, 338, 2018.